Comprehensive study of $d + {}^{6}$Li via observing simultaneous outgoing neutrons, γ rays, and charged particles

S. N. Paneru,* H. Y. Lee,† C. Prokop, S. A. Kuvin, C. Fichtl, P. Gastis, G. M. Hale, E. Leal-Cidoncha, M. Mosby, and M. Paris
Los Alamos National Laboratory, Los Alamos, New Mexico 87545, USA

M. Febbraro
Air Force Institute of Technology, Wright-Patterson AFB, Ohio 45433, USA and Oak Ridge National Laboratory, Oak Ridge, Tennessee 37830, USA

T. T. King, J. Nattress, and T. J. Ruland
Oak Ridge National Laboratory, Oak Ridge, Tennessee 37830, USA

R. J. deBoer, E. Stech, T. Bailey, C. Boomershine, S. Carmichael, A. Clark, R. Fang, J. Görres, R. Kelmar, K. Lee, K. Manukyan, M. Matney, J. McDonaugh, A. Miller, A. Nelson, P. O'Malley, D. Robertson, Shahina, W. Tan, W. W. von Seeger, and M. Wiescher
University of Notre Dame, Notre Dame, Indiana 46556, USA

A. Roberts
Department of Physics, University of Colorado Denver, Denver, Colorado 80204, USA

(Received 1 July 2024; revised 25 August 2024; accepted 24 September 2024; published 10 October 2024)

Deuteron-induced reactions on ^{6}Li are important for nuclear structure studies and nuclear applications. A new experimental effort was dedicated to improve incomplete partial cross sections and the angular distribution information for $d + {}^{6}$Li reactions and to address the inconsistencies between various R-matrix evaluations of the ^{8}Be system. The new measurements were performed over a deuteron energy range of 1.8 to 10 MeV with an angular distribution coverage of 20°–170° for outgoing particles. The experiment simultaneously measured neutrons, charged particles, and γ rays from the various exit channels of the $d + {}^{6}$Li reaction. The cross sections for open reaction channels measured simultaneously are presented. In addition, results for the ^{6}Li(d, n) ^{7}Be total cross section using the activation method are also presented.

DOI: 10.1103/PhysRevC.110.044603

I. INTRODUCTION

Due to their relevance to nuclear astrophysics and for thermal reactor designs, charged-particle-induced reactions on light nuclei such as ^{6}Li(d, p), ^{6}Li(d, n), ^{6}Li$(^{3}$He$, n)$, ^{6}Li(d, α), and ^{7}Li(d, p) have been widely studied [1–22]. Early studies involved measuring the neutron transfer reactions on 1 p shell nuclei, providing (d, p) angular distribution data at an incident energy of 12 MeV, for a better understanding of the optical model and the structure of light nuclei through comparison with nuclear shell model calculations [23]. This was followed by measurements at energies between 4.5–6 MeV to investigate the interplay between distorted wave theory and a compound nucleus background using the Hauser-Feshbach theory [13]. Besides using techniques to directly measure the angular distributions of outgoing particles, the activation method was often used to count decays of radioactive daughter nuclei to deduce cross sections with high precision at deuteron energies less than 1 MeV [5]. Measurements in this energy range were of high importance in characterizing "big bang" nucleosynthesis of light nuclei. Measurements continue to be performed to try to resolve the so-called "lithium abundance problem" by improving the associated nuclear data [24]. Other applications include the use of ^{6}Li(d, n) and ^{7}Li(p, n) as potential sources of intense neutron beams and for tritium breeding using "lithium blankets" in fusion energy applications [25,26].

For the case of $d + {}^{6}$Li, the compound nucleus is ^{8}Be, and the reactions are modeled using R-matrix theory [29] at deuteron energies below the breakup channel and Hauser-Feshbach theory at high energy for evaluations [30]. The effort of in-depth study on the ^{8}Be system has incorporated tens of experimental reaction mechanisms with light elements [31], to test data consistency by way of resonance matrix analyses. However, the resulting description of the $d + {}^{6}$Li reactions is far from complete because experimental data have

*Contact author: paneru@lanl.gov
†Contact author: hylee@lanl.gov

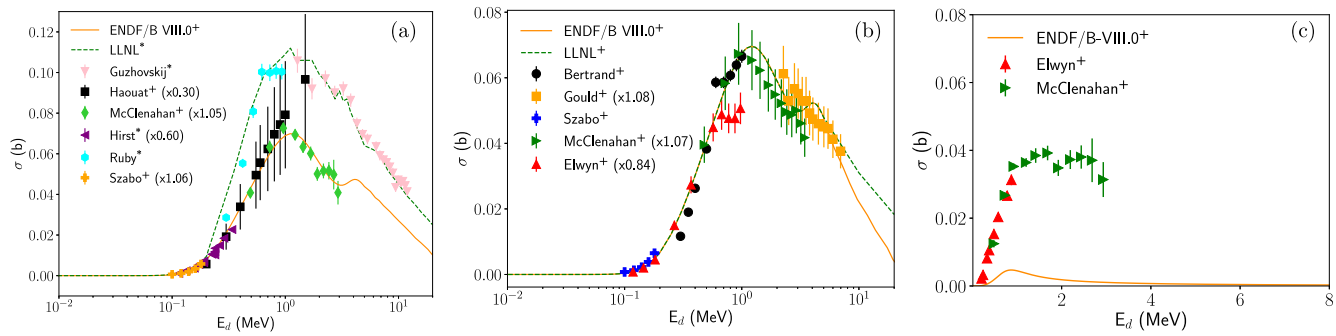

FIG. 1. Integrated cross sections for (a) ^{6}Li$(d,n)^{7}$Be, (b) ^{6}Li$(d,p_0)^{7}$Li$_{gs}$, and c) ^{6}Li$(d,n_1)^{7}$Be$_{ex}$. Symbols + and ∗ represent the partial and production cross section for each reaction channel, respectively. In (a), the orange solid line is ENDF/B-VIII.0 [27], which only includes the ^{6}Li$(d,n_0)^{7}$Be data. The green dashed line is the LLNL evaluation [28], which includes only the sum of the ^{6}Li$(d,n_0)^{7}$Be$_{gs}$ and ^{6}Li$(d,n_1)^{7}$Be$_{ex}$ cross sections. Data from Ruby *et al.* [6], Hirst [8], and Guzhovskij *et al.* [7] are ^{7}Be production cross sections, while the data from Haouat [9], McClenahan and Segel [2], and Szabó *et al.* [5] are direct measurements of the ^{6}Li$(d,n_0)^{7}$Be$_{gs}$ partial cross section. In (b), data from Bertrand *et al.* [3], Could *et al.* [4], Szabó *et al.* [5], McClenahan and Segel [2], and Elwyn *et al.* [1] are direct measurements of ^{6}Li$(d,p_0)^{7}$Li$_{gs}$ partial cross sections. The multiplicative factors for each data set shown in the legend come from the *R*-matrix analysis parameters in the ENDF/B-VIII.0 evaluation files. In (c), the ^{6}Li$(d,n_1)^{7}$Be cross section data from Elwyn *et al.* [1] and McClenahan and Segel [2] are compared with ENDF/B-VIII.0, which underestimates the experimental data by an order of magnitude.

limited energy ranges and incomplete differential cross section information.

One main motivation in this work is to obtain new, independent experimental data for deuteron induced reactions on lithium to resolve an inconsistency among different evaluation libraries, which are implemented directly into Monte Carlo transport codes for many nuclear applications. The ENDF/B-VIII.0 evaluation [27,32] only includes ^{6}Li$(d,d)^{6}$Li$_{gs}$, ^{6}Li$(d,\alpha_0)\alpha$, ^{6}Li$(d,n_0)^{7}$Be, and ^{6}Li$(d,p_0)^{7}$Li partial cross sections, where the latter two are consistent on the basis of mirror-symmetry and accurately reproduce the experimental data of Refs. [1–5,8,9]. A major criticism of the ENDF/B-VIII.0 evaluation stems from the lack of information regarding other open reaction channels, such as ^{6}Li$(d,n_1)^{7}$Be, ^{6}Li$(d,p_1)^{7}$Li, and transfer reactions to higher excited states in the residual nuclei that are particle unbound (e.g., to triton emission). This is illustrated in Figs. 1(a) and 1(c), where the lack of (d,n_1) data in the evaluation results in an under-prediction for ^{7}Be production. The results from *R*-matrix analysis of reactions forming a compound ^{8}Be system using energy dependent analysis (EDA) *R*-matrix code are reported in the ENDF/B-VIII.0 evaluation. Although EDA includes reaction channels to higher excited states in residual nuclei, the analysis does not include data to constrain the *R*-matrix fits. Hence, the partial cross sections for ^{6}Li$(d,n_1)^{7}$Be and ^{6}Li$(d,p_1)^{7}$Li reactions are underpredicted [see Fig. 1(c)] and were not reported to the ENDF/B-VIII.0 evaluation. A more recent LLNL *R*-matrix analysis [28] uses the ^{7}Be production data to derive the ^{6}Li$(d,n)^{7}$Be cross section, but still derives the ^{6}Li$(d,p)^{7}$Li cross section from ^{6}Li$(d,p_0)^{7}$Li partial cross section data [see Fig. 1(b)]. Thus, there is an inconsistency in the description of (d,p) and (d,n) production cross section and partial cross section data in the LLNL evaluation, while both libraries also do not sufficiently describe all of the open reaction channels. An additional concern is raised on how experimental data sets were utilized to calculate evaluated cross sections consistently. The normalization factors that were applied to different data sets were varied from 0.3 to 1.07, many outside quoted uncertainties and without any detailed justifications.

From a practical standpoint, the current ENDF/B-VIII.0 evaluation not only underpredicts ^{7}Be production but also neutron, tritium, and other charged particle production, particularly at energies above 2 MeV. As an example, the (d,n_2) reaction to the particle unbound second excited state in ^{7}Be will break up through the emission of an alpha particle and ^{3}He (in addition to the lower energy neutron, with respect to populating the groundstate, in the exit channel). Meanwhile, the (d,p_2) reaction to the second excited state in ^{7}Li will break up through the emission of an alpha particle and a triton. Hence, it is important to consider the different reaction mechanisms that can contribute to different particle production.

The inconsistencies between both evaluated and experimental data and the lack of sufficient differential data motivate new measurements over a broad energy range. This work provides correlated outgoing neutron angular distributions over the full ENDF energy range benefiting both future *R*-matrix analysis and producing a more complete set of data for the partial cross sections that are lacking in the current evaluation of $d+{}^{6}$Li. We also simultaneously measured the outgoing charged particle channels and γ-ray transitions. Using secondary γ-rays, angle-integrated partial cross sections are also experimentally determined.

II. EXPERIMENT

A. Measurement details

The experiment was performed at the University of Notre Dame Nuclear Science Laboratory using the FN 10 MV Tandem Accelerator. A deuteron beam with energies ranging from 1.8 to 15.0 MeV was made incident on a metallic enriched ^{6}Li targets, with a 200 μg/cm^2 nominal thickness. ^{6}Li targets were prepared using the vacuum evaporation technique. Carbon foils with a thickness of μg/cm^2 (Arizona Carbon Foil

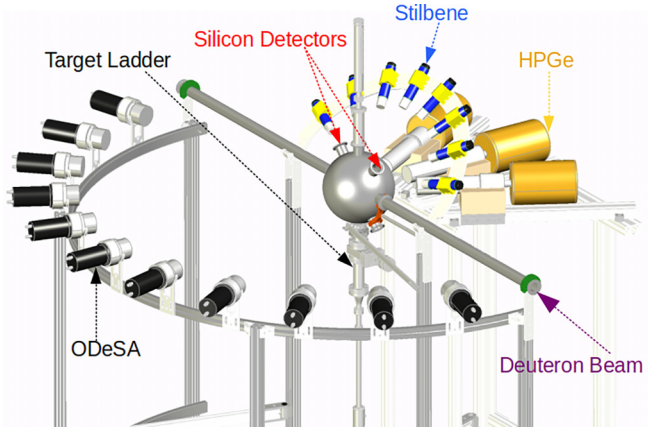

FIG. 2. 3-D model of experimental setup showing the low mass spherical chamber and frame as well as locations of the neutron detectors (ODeSA and stilbene), silicon charged particle detectors, and HPGe detectors used for γ-ray detection.

Co., Inc.) were used as backings. Enriched ^{6}Li was placed in a tantalum boat as the evaporation source. The evaporation process was conducted at a base pressure of 3×10^{-6} torr. The distance between the tantalum boat and the foils was set at 20 cm to ensure uniform deposition and to minimize the heating of the backings. The Li deposition was monitored using gold-coated quartz crystals and recorded by a thickness monitor. The evaporation rate was maintained at 0.2 μg/min. After evaporation, the targets were allowed to cool for 60 minutes, after which high-purity argon gas was slowly introduced into the evaporator. The targets were then transferred to the beam line using an argon-filled glove box to prevent oxidation. The uncertainties in target thickness prepared from this technique is ≈10%.

The experimental setup is shown in Fig. 2. The target was placed inside a 10 in. diameter low-mass aluminum spherical vacuum chamber that was designed to reduce unwanted neutron scattering and γ-ray attenuation. The supporting frame was constructed with light mass aluminum, to reduce neutron scattering and room returns as potential ambient backgrounds. The target was placed in a target ladder made up of aluminum, operated from the bottom of the chamber, which allowed for the mounting of three ^{6}Li targets. A beam tuning ladder was operated from the top of the chamber, which included the beam defining collimator used to define the desired beam spot (approximately 5 mm in diameter) and to mount a reference CD_2 target. During experiments, the deuteron beam current intensity was measured by a Faraday cup, located 2 m downstream from the target and electrically isolated from the rest of beam line. The beam stop was a carbon plate which was shielded to suppress beam induced background.

The experimental setup was designed to detect neutrons, γ rays, and charged particles simultaneously. Neutrons were detected with two arrays made up with different types of detectors. The neutron array consisted of ten detectors from the ORNL Deuterated Spectroscopic Array (ODeSA) [33] and was used to measured neutrons at the laboratory angles from 28.3° to 164.8°, while the other neutron array of eight 1 in. × 1 in. cylindrical stilbene detectors covered the laboratory angular range from 20° to 160°. The ODeSA detectors were placed at a distance of 100 cm, while stilbene detectors were placed at a distance of 33 cm from the center of the chamber, so that their geometric efficiencies were similar. Charged particles were detected using two sets of silicon detector telescopes placed at the laboratory angles of 45° and 135°. Each detector telescope was comprised of three surface silicon barrier detectors (SSBs with 500 μm thickness to serve as a $\Delta E1$-$\Delta E2$-E) placed coaxially with a distance of 112 mm from the target. The absolute efficiency and energy calibration of the silicon detectors were determined using an ^{241}Am source. Secondary γ rays from deexcitation transitions in ^{7}Be, ^{13}C, ^{13}N, and ^{17}F were observed using high purity germanium (HPGe) detectors placed at 45°, 90°, and 135°. These HPGe detectors were previously part of the GEANIE array [34–36], which was used extensively for studying the neutron-induced γ rays produced via (n, n') and $(n, 2n)$ reactions at the Los Alamos Neutron Science Center. Their intrinsic efficiencies varied from 20% to 25% [37]. For in-beam data, photomultiplier tube (PMT) outputs from neutron detectors and HPGe detectors as well as preamplifer outputs from each SSB detector were fed into multiple CAEN V1730 digitizers. Each CAEN V1730 waveform digitizer recorded detector signals at a sampling rate of 500 MS/s with 14-bit resolution. The neutron and accelerator timing buncher reference times were recorded with PSD firmware while the HPGe and silicon detector signals were recorded on V1730s with the PHA firmware. The beam from the FN accelerator was bunched with a frequency of 400 ns. The time-of-flight (TOF) method was applied for ODeSA detectors by taking the neutron's arrival time relative to the accelerator buncher timing. This provided additional information about the neutron's energy in addition to that obtained from ODeSA's spectrum unfolding technique.

Activation runs were performed at deuteron energies between 2 and 15 MeV and at a proton energy at 3.5 MeV [to check against the ^{7}Li$(p, n)^{7}$Be reaction]. Typical beam intensities were 200 nA on target. Targets for activation runs were produced by evaporating enriched ^{6}LiF material onto beam stop carbon backings of thicknesses ranging from 0.5 to 2 mm and had nominal Li thicknesses of 200 μg/cm^2 (<20 keV energy loss). A target of natural isotopic abundance was also used for normalization purposes with the activation on ^{7}Li(p, n). Carbon backings were used in order to avoid the production of long lived radioactive isotopes from the backing. The offline activation setup was composed of one well-calibrated HPGe detector and the reproducible multi-target position cell, inside the lead castle made up of 8 in. of lead with a 1/4 in. internal layer of copper and with the dimensions of $2 \times 2 \times 3$ ft^3.

B. Targets and relative normalization

To reduce neutron backgrounds from ^{19}F(d, n), metallic lithium targets were chosen for this measurement, instead of commonly used LiF targets. High purity ^{6}Li was thermally evaporated to a carbon backing, then the targets were transferred from the evaporator to the chamber with an effort

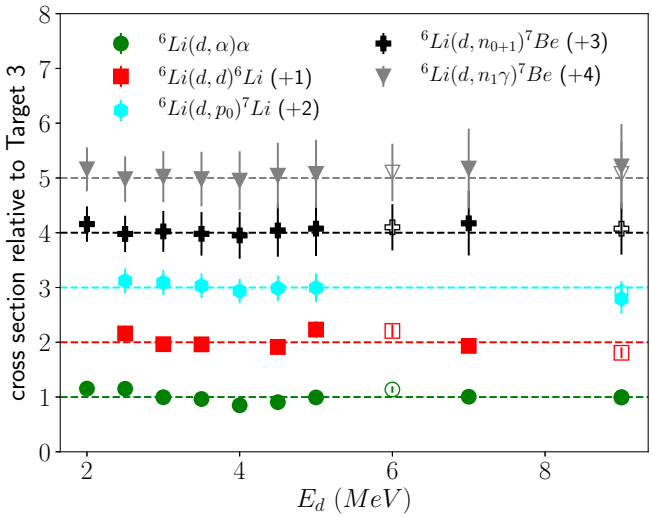

FIG. 3. The ratio of cross sections determined from targets 1 and 2 relative to target 3 for different reaction channels. The solid and open markers represent targets 1 and 2, respectively. The numbers in the parentheses are vertical offsets added to the original ratio values for easy visualization.

to minimize any oxygen exposure. However, three targets showed different oxygen contaminants and different ^{6}Li contents. The first two targets ("target 1" and "target 2") were used to provide relative cross sections (or shape data) and "target 3" was used for deducing absolute cross sections. Cross sections measured with targets 1 and 2 were normalized to those of target 3, using the reference reaction of $^6\mathrm{Li}(d,\alpha)\alpha$ and the reaction $^6\mathrm{Li}(d,p_0)^7\mathrm{Li}$ as a consistency check. Since the oxidation of target 1 was observed, the measurements at $E_d = 2.0$ and 2.5 MeV were used to provide relative normalization for target 1. The ratio of yields per unit integrated charge for the same silicon detector telescope at the same E_d was used to find the normalization n:

$$n \times \frac{Y_i}{Q_i} = \frac{Y_{\mathrm{ref}}}{Q_{\mathrm{ref}}}, \tag{1}$$

where Y_i is the α yield or p_0 yield for target i and Q_i is the integrated charge for a measurement with target i, and $i = 1, 2$. Similarly, Y_{ref} is the α yield or p_0 yield for the reference target and Q_{ref} is the integrated charge for a measurement with a reference target. The relative normalization factors for targets 1 and 2 were determined to be 1.18 ± 0.06 and 2.53 ± 0.07. The ratio of cross sections determined from targets 1 and 2 relative to target 3 is presented in Fig. 3. The results from these targets, after relative normalization corrections, became consistent with the results from the uncorrected target 3.

Since the uncertainties in target thickness for ^{6}Li targets made from the evaporation technique is about 10%, we determined the thickness of ^{6}Li targets by renormalizing our $^6\mathrm{Li}(d,n)^7\mathrm{Be}$ cross section to the cross sections obtained from the activation method (see Sec. III B 2). The absolute value of target thickness is determined by minimizing the χ^2 between the activation data and the data from neutron detectors at overlapping deuteron beam energies. The thickness for target 3 from this approach was determined to be 192.6 μg/cm^2 with an uncertainty of 5%, which is quoted as systematic uncertainty in Table I.

TABLE I. Estimation of systematic uncertainties

	Error		
Source of error	Charged particles	Gammas	Neutrons
Target thickness (rel.)	5.0%	5.0%	5.0%
Beam properties	1.9%	1.9%	1.9%
Yield calculation	1.0%	1.0%	4.0%
Absolute efficiency	0.9%	2.9%	5.0%
Total	5.51%	6.16%	8.34%

C. Systematic uncertainties

The uncertainties presented in this study include statistical errors only. The contribution of systematic errors have been discussed in each section. The systematic error associated with target thickness and the beam properties are common to all results from this work. The number of incident beam particles is determined from the integrated charge, the uncertainty for which is estimated to be 3.5%, and this is applied as statistical error to our data. Similarly, the systematic uncertainty arising from fluctuations in beam intensity and different beam tuning is estimated to be 1.9%. The yield for reaction product of interest was determined by integrating the counts under the peak of interest after proper background subtraction whenever necessary. Background subtraction is carried out using usual the fitting procedures and are described briefly in Sec. III. The errors from the background subtraction are propagated to determine the statistical error on yields. The systematic uncertainties for yield calculation and absolute detection efficiency determination for different detectors will be further discussed in Sec. III B. Absolute detection efficiency here is defined as the product of intrinsic efficiency and the solid angle. Total systematic uncertainties of 5.5%, 6.2%, and 8.3% are estimated for charged particle exit channels, for γ-ray angular distributions, and for neutrons in exit channels, respectively. Total systematic uncertainties reported here are for results from target 3 only. The systematic uncertainties from this work are summarized in Table I.

III. ANALYSES AND RESULTS

Differential cross sections were obtained for charged particle reactions on ^{6}Li for reactions such as (d,d), (d,α), and (d,p) as described in Sec. III A. The neutron production from $^6\mathrm{Li}(d,n)$ will be presented for the total cross section using the activation method, and for differential cross sections using the neutron spectrum unfolding method in Sec. III B. γ-ray production cross sections will be discussed for the $^6\mathrm{Li}(d,n_1)$ reaction in Sec. III C. In Sec. III D, results from the reference reaction $d(d,n)$ will be discussed. The results from R-matrix analysis including data from this work are compared with the ENDF/B VIII.0 evaluation in Sec. III E.

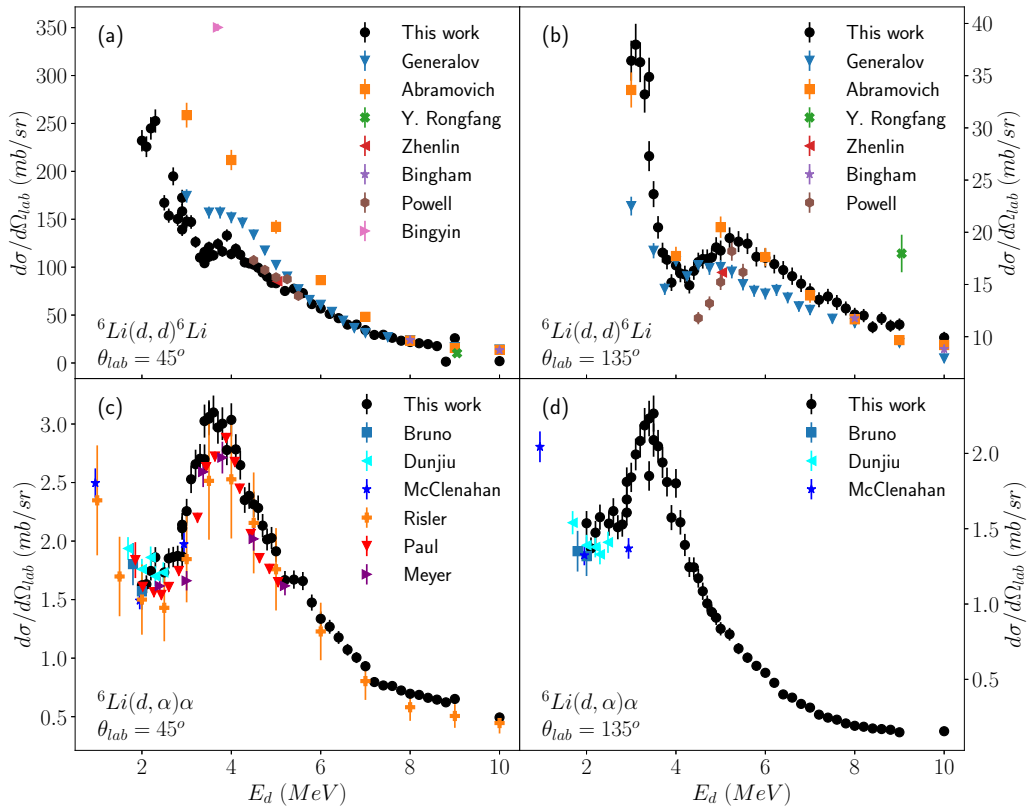

FIG. 4. Differential cross sections for ^{6}Li(d, d) at (a) $\theta_{\rm lab} = 45^\circ$ and (b) $\theta_{\rm lab} = 135^\circ$, and for ^{6}Li$(d, \alpha)\alpha$ at (c) $\theta_{\rm lab} = 45^\circ$ and (d) $\theta_{\rm lab} = 135^\circ$. The results from this work are compared to literature data labeled as Generalov [11], Abramovich [12], Y. Rongfang [14], Bingyin [21], Zhelin [15], Bingham [16], Powell [13], Risler [18], Bruno [17], Paul [19], Meyer [20], Dunjiu [31], and McClenahan [2].

A. Charged particle reactions

Charged particle reaction products from ^{6}Li $+d$ were detected by two silicon detector telescopes as described in Sec. II. Our results were compared with literature data taken from EXFOR [31]. In cases where the uncertainties in the literature data were not provided, the upper limits on the relative uncertainty presented in the corresponding publications were adopted. For all charged particle channels, the yield under the peak of interest was determined after background subtraction, where we fit the peak of interest and the underlying background with common fitting functions. The fit parameters were then varied by their standard deviation to determine the variance of the yield. For isolated peaks, for example that corresponding to the ^{6}Li$(d, \alpha)\alpha$ reaction, the area was found by summing bin by bin to determine the yield and then compared to the fitting procedure. Following this procedure, the systematic uncertainty for the yield calculation for charged particles was determined to be at most 1%. The absolute detection efficiencies of the silicon detectors were determined using the activity of a ^{241}Am source. The systematic uncertainty in absolute detection efficiency of the silicon detectors was estimated to be 0.9%.

1. ^{6}Li$(d, d)^6$Li

The elastic scattering cross sections of ^{6}Li(d, d) at $\theta_{\rm lab} = 45^\circ$ and 135° are presented in Figs. 4(a) and 4(b) along with the results from the literature. Differential cross sections for the backward angle of 135° could not be measured below $E_d = 2.8$ MeV as the elastic scattering peak lies too close to the detector's threshold. The differential scattering cross section results from Generalov *et al.* [11] have random uncertainties of 5–10% and a systematic uncertainty of 4%. For comparison to our results, we used 10% uncertainty on the Generalov *et al.* [11] data points. We used 5% relative uncertainties on the ^{6}Li$(d, d)^6$Li data from Bingham *et al.* [16]. Similarly, relative uncertainties of 4% and 5% were assumed for data from Zhenlin *et al.* [15] and Powell *et al.* [13]. The results from this work at $\theta_{\rm lab} = 45^\circ$ [see Fig. 4(a)] are in good agreement with data from Refs. [13,14,16]. At $E_d < 5.5$ MeV, the data from Generalov *et al.* [11] show a similar shape for the excitation function, while the magnitude is higher compared to our results. We do not agree with the data from Abramovich *et al.* [12] and Bingyin *et al.* [21]. Our results at $\theta_{\rm lab} = 135^\circ$, shown in Fig. 4(b), are consistent with data from Refs. [12,15,16] and in fair agreement with data from Generalov *et al.* [11] except for over the energy range from $E_d = 5$–7 MeV. The shape of the data from Powell *et al.* [13] and Yuan Rongfang *et al.* [14] are different compared to most of the other data sets. Before this work, there were essentially two measurements, those of Abramovich *et al.* [12] and Generalov *et al.* [11], to cover the entire energy range from $E_d = 1.8$–10 MeV. Our results are consistent with those of Abramovich *et al.* [12] at $\theta_{\rm lab} = 135^\circ$, but they differ

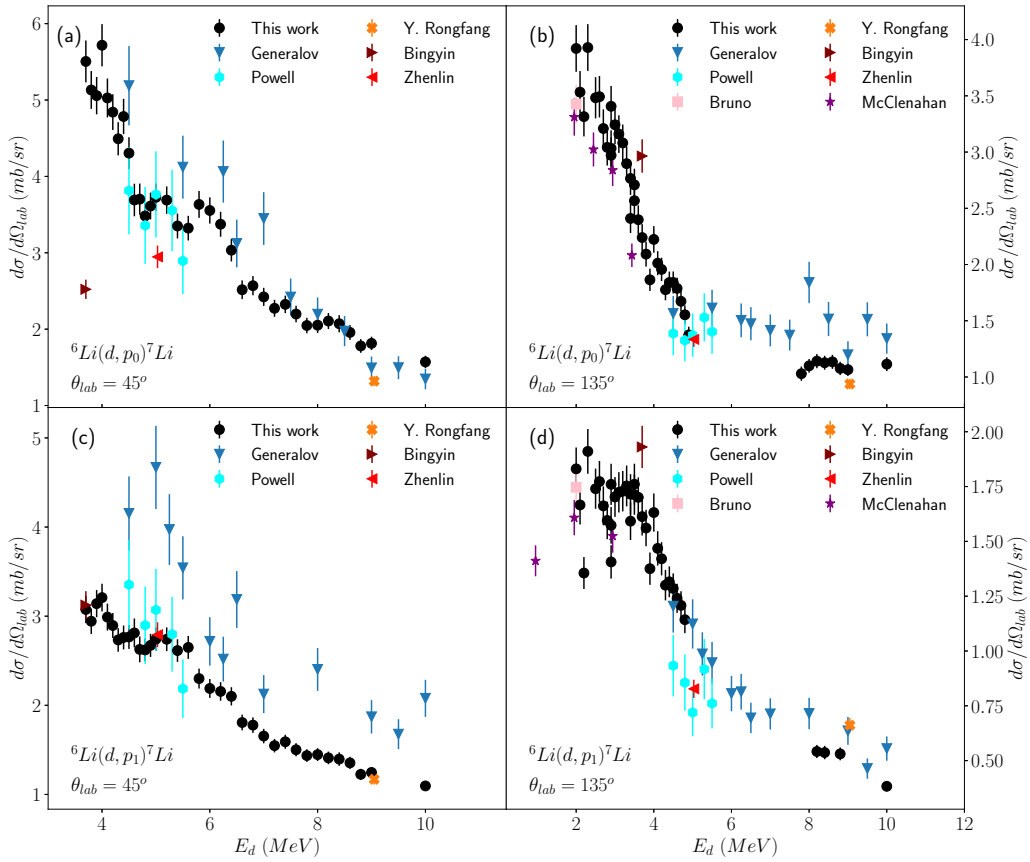

FIG. 5. Differential cross sections for the ^{6}Li$(d, p_0)^7$Li reaction at (a) $\theta_{\rm lab} = 45^\circ$ and (b) $\theta_{\rm lab} = 135^\circ$ and for the ^{6}Li$(d, p_1)^7$Li reaction at (c) $\theta_{\rm lab} = 45^\circ$ and (d) $\theta_{\rm lab} = 135^\circ$. The results from this work are compared to literature data labeled as Generalov [38], Powell [13], Y. Rongfang [14], Bingyin [21], Zhelin [15], Bruno [17], and McClenahan [2].

significantly with both previous measurements at $E_d < 6.0$ MeV at $\theta_{\rm lab} = 45^\circ$.

2. ^{6}Li$(d, \alpha)\alpha$

The differential cross section for the ^{6}Li$(d, \alpha)\alpha$ reaction was determined from this work, the results of which are presented in Figs. 4(c) and 4(d). Since we have two identical α particles in the outgoing channel, the yield is divided by a factor of 2 to report the reaction cross section for the ^{6}Li$(d, \alpha)\alpha$ reaction. The angular distribution for ^{6}Li$(d, \alpha)\alpha$ must be symmetric around $\theta_{\rm c.m.} = 90^\circ$ due to the fact that we have identical particles in the exit channel. The shapes of excitation functions presented in Figs. 4(c) and 4(d) are similar. The differential cross section is enhanced around $E_d = 3.5$ MeV for both at $\theta_{\rm lab} = 45^\circ$ and $\theta_{\rm lab} = 135^\circ$ corresponding to the 2^+ resonance state at ≈25.2 MeV in ^{8}Be. Our fine energy-bin data observed a slight enhancement around $E_d = 5.4$ MeV at $\theta_{\rm lab} = 45^\circ$. Bruno *et al.* [17] reported angular distributions at $E_d = 1.0$ and 2.0 MeV as the α production angular distributions and they were divided by a factor of two for consistent comparison with our data. The data of Paul and Lieb [19] were also divided by a factor of two for the same reason. The results from this work are consistent with previous measurements from Refs. [2,17–20,31] at both $\theta_{\rm lab} = 45^\circ$ and $\theta_{\rm lab} = 135^\circ$.

3. ^{6}Li$(d, p)^7$Li

The differential cross sections for ^{6}Li$(d, p_0)^7$Li and ^{6}Li$(d, p_1)^7$Li reactions determined from this work are presented in Fig. 5. For the detector at $\theta_{\rm lab} = 45^\circ$, there were protons that punched through the $\Delta E1$ detector but did not get detected in the $\Delta E2$ detector, due to the detector's intrinsic threshold and the dead layer on the SSB detectors. Therefore, data below $E_d = 3.7$ MeV were not recorded in the results for both ^{6}Li(d, p_0) and ^{6}Li(d, p_0) reactions [Figs. 5(a) and 5(c)]. At $\theta_{\rm lab} = 135^\circ$, for the same reason described above, there were no data recorded for $E_d = 5$–8 MeV [Figs. 5(b) and 5(d)]. This work was found to be fairly consistent with previous measurements for both (d, p_0) and (d, p_1) with few exceptions. At $\theta_{\rm lab} = 45^\circ$, results from Generalov *et al.* [38] were systematically higher compared to this work. In general the results from Refs. [2,13–15] were consistent with this work. The results from Bingyin *et al.* [21] were consistent with results from this work except for the ^{6}Li$(d, p_0)^7$Li reaction at $\theta_{\rm lab} = 45^\circ$. Another independent measurement would

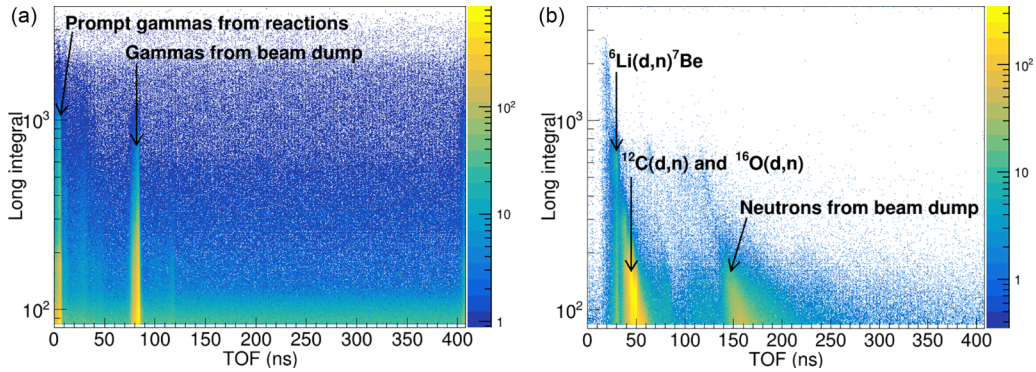

FIG. 6. (a) Gamma gated spectrum for TOF vs long integral. (b) Neutron gated spectrum for TOF vs long integral.

be desired to sort out the differences between the results from this work and from Generalov *et al.* [38].

B. ^{6}Li$(d, n)^{7}$Be

1. Neutron spectrum unfolding method

Neutron angular distributions for the ^{6}Li$(d, n)^{7}$Be reaction were measured using the ODeSA detectors [33]. Neutrons were separated from γ-rays using the conventional pulse shape discrimination (PSD) technique. A light output threshold of 300 keVee was chosen for the ODeSA detectors, leading to a clear separation of neutrons form γ rays with a figure of merit >2.5. Once neutrons were identified, an additional TOF cut was applied to select neutron energies relevant to specified reaction kinematics. Plots of TOF vs the long integral for neutrons and γ rays are shown in Fig. 6. In Fig. 6(a), the strong line around 80 ns was associated with the γ rays originating from the beam dump. In Fig. 6(b), the first few lines, starting at around 30 ns, were associated with neutrons from the deuteron induced reactions on ^{6}Li, ^{12}C, and ^{16}O. The region around TOF $\approx$ 80 ns is associated with the γ rays from the beam dump leaking into our neutron gate, which is negligible as seen in Fig. 6(b). The second peaks, starting around $\approx$ 150 ns, were found to be background neutrons from the beam dump, a major contributor to our neutron background.

The neutrons of interest (10 < TOF < 80 ns) are clearly separated from the background neutrons from the beam dump (TOF $\approx$ 150 ns), as seen in Fig. 7(a). The maroon solid lines include all the neutrons produced from the target, referred to as a wide gate hereafter, while the dotted green lines include the neutrons only from the ^{6}Li$(d, n)^{7}$Be reaction, referred to as a narrow gate hereafter. The TOF gated neutron spectra are analyzed using the technique of spectrum unfolding as described by Febbraro *et al.* [39]. The spectra unfolding technique converts the light output spectra into the neutron energy spectra as shown in Figs. 7(b) and 7(c). The dotted lines represent the expected kinematic positions for the reactions ^{6}Li$(d, n_0)^{7}$Be, ^{6}Li$(d, n_1)^{7}$Be, ^{12}C$(d, n_0)^{13}$N, and ^{16}O$(d, n_0)^{17}$F. The narrow TOF gate on the region of interest removes the background contribution from other reaction channels as shown in Fig. 7(c). The kinematically close neutron peaks corresponding to ^{6}Li$(d, n_0)^{7}$Be and ^{6}Li$(d, n_1)^{7}$Be were not resolved for ODeSA detectors with the spectrum unfolding method. The timing resolution for ODeSA detectors was determined to be 4.2 ns at full width half maximum. Also, the ^{6}Li$(d, n_0)^{7}$Be and ^{6}Li$(d, n_1)^{7}$Be reactions could not be separated using a TOF method for all deuteron beam energies due to insufficient timing resolution to separate 429 keV neutrons at the flight length of 100 cm. Stilbene detectors used in the experiment have a better timing resolution of 3.26 ns at full width half maximum, but they were placed only 33 cm away from the target. We applied the neutron spectrum

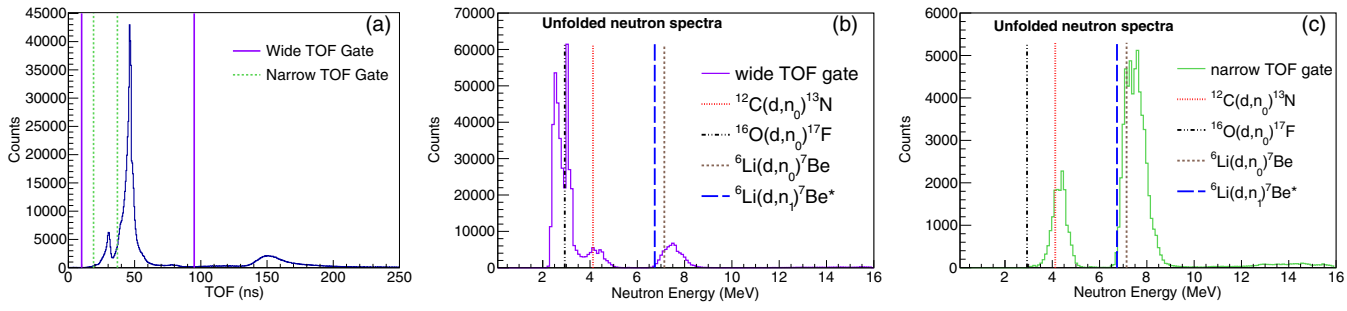

FIG. 7. (a) TOF spectra for neutrons for an ODeSA detector placed at $\theta_{\text{lab}} = 59.7^{\circ}$ for $E_d = 5.0$ MeV. The purple solid lines represent the wide gate while the green dashed lines represent the narrow gate. (b) Unfolded neutron spectra under the wide TOF cut. (c) Unfolded neutron spectra under the narrow TOF cut. The dotted brown and blue lines represent the expected kinematic positions for ^{6}Li(d, n_0) and ^{6}Li(d, n_1), respectively. The dotted red and pink lines represent the kinematic positions for ^{12}C(d, n_0) and ^{16}O(d, n_0).

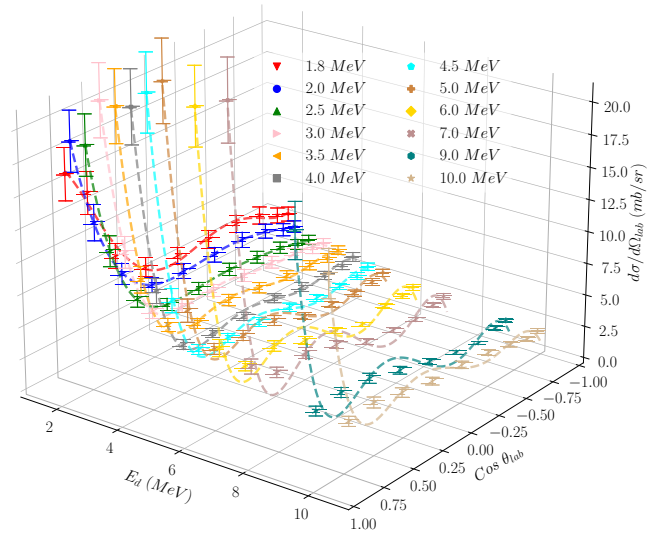

FIG. 8. Neutron angular distributions of the ^{6}Li(d, n_{0+1}) reactions for a given incident deuteron beam energy, E_d, measured with the ODeSA detectors. The dashed lines are Legendre polynomial fits to the data.

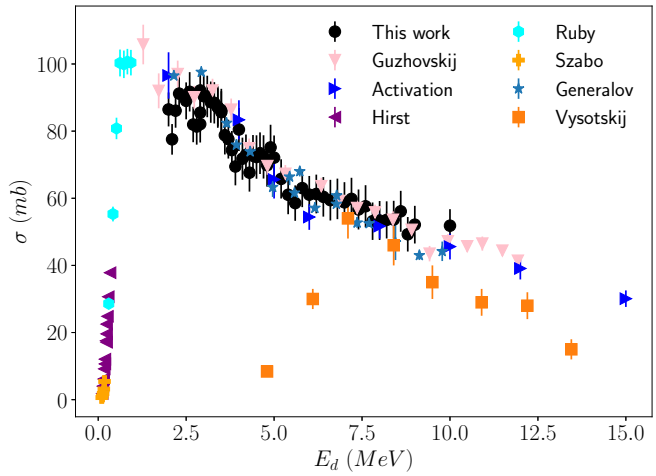

FIG. 9. Cross sections for the ^{6}Li$(d, n_{0+1})^7$Be reaction. The angle-integrated cross sections were deduced from neutron angular distributions measured with the ODeSA detectors labeled as "This work". The results from the activation method from this work are labeled as "Activation". Both results show good agreement with the other data from the literature, which are labeled as Guzhovskij [7], Hirst [8], Ruby [6], Szabo [5], Generalov [10], and Vysotskij [40].

unfolding technique to neutron spectra with the simulated detector response matrix, which are yet to be validated from measurements. So, the results from the stilbene detectors are not presented in this paper.

The total yields for ^{6}Li$(d, n_{0+1})^7$Be are obtained from the unfolded spectra after background subtraction whenever necessary. The neutron detection efficiency curve of the ODeSA detectors was taken from Fig. 8 of Ref. [33]. The uncertainties in the neutron detection efficiency were quoted between 5% and 10% for the neutron energy range of $E_n = 3.2$–15.5 MeV. This uncertainty is statistical in nature and propagated to the cross section uncertainties. Measured neutron angular distributions for different deuteron beam energies are shown in Fig. 8. The angular distributions were fitted with Legendre polynomials, which were used to deduce the angle-integrated cross sections. The angle-integrated cross sections from this work are compared with those from the literature in Fig. 9. Our results were found to be consistent with previous measurements from Refs. [5–8,10,40]. The drop in cross section below $E_d = 7$ MeV observed by Vysotskij *et al.* [40] was not seen in other measurements.

The uncertainty estimates for neutron spectrum unfolding method are discussed below.

(i) Neutron background: The major source of neutron background in this experiment comes from the those produced from the beam impinging on the beam dump. These neutrons are separated using the time-of-flight cuts. Another source of background neutrons comes from the breakup of the deuteron beam. However, a phase space of these breakup neutrons does not overlap with the neutrons of interest. Thus, the systematic uncertainty in the neutron yield calculation due to background is <1%.

(ii) Efficiency of ODeSA detector: The intrinsic efficiency of the ODeSA detectors was measured using neutrons generated from the ^{9}Be(d, n) reaction on a thick-target using TOF [33]. This reaction was very well characterized [41,42] but was limited to the neutron energy range between ≈0.5 and 5 MeV. The measured efficiencies have uncertainties ranging from 5% at the lower energies up to greater than 10% at the highest energies. A MCNP simulation was developed to validate the measured efficiency and extend the intrinsic efficiency to neutron energies higher than 5 MeV. The adjusted intrinsic efficiency curve was obtained after applying correct light output thresholds. Statistical uncertainty of 10% and systematic uncertainty of 5% are estimated for intrinsic efficiency of ODeSA detectors.

(iii) Neutron unfolding systematics: We used the maximum-likelihood expectation maximization (MLEM) method [39,43] to unfold the neutron spectra. The uncertainty due to a number of optimal iterations was determined to be less than 1% by studying the neutron yield for a neutron peak of interest with the variation in the number of iterations. Variations in the neutron response matrix for the ODeSA detector were obtained by varying the non-zero elements of the neutron response matrix uniformly by an arbitrary percentage, x, to create a new response matrix, which was fed into the unfolding algorithm. The exercise was repeated for 1000 iterations to measure the variance in neutron yield estimates. For $x = 6\%$, the variance in the yield estimates was determined to be 4%, which has been quoted as a systematic uncertainty for this work. The value of x was chosen such that the

reduced χ^2 of the yield estimates from the yield value before randomization was ≈1. The total systematic uncertainty for the neutron yield calculations was estimated to be 4%.

2. Activation method

The ^{6}Li$(d,n)^{7}$Be reaction cross section was determined using the activation technique by counting the 478 keV characteristic γ-ray from the decay of ^{7}Be into ^{7}Li via electron capture. Although a significant amount of short-lived (10 minute half-life) ^{13}N was produced from the ^{12}C$(d,n)^{13}$N reaction, clean γ-ray spectra were obtained by waiting about 3.3 hours (20× ^{13}N half-life) from the end of each activation run before starting the γ-ray counting. To minimize systematic uncertainties, the cross section was determined relative to that of the ^{7}Li$(p,n)^{7}$Be reaction and using a lithium target of natural isotopic abundance [^{7}Li: 92.41(4)%; ^{6}Li: 7.59(4)%] at a proton energy of 3.5 MeV. The evaluation by Liskien and Paulsen [44] listed the ^{7}Li$(p,n)^{7}$Be cross section as 282.5 or 290 mb, depending on the method of calculation. The 5% overall uncertainty, quoted for the 0-degree cross section compilation, was also assumed for that of the total cross section. By taking the ratio of the cross sections that produce the same γ ray, the absolute detection efficiency cancels out. Uncertainties are then dominated by statistics in counts, the reference ^{7}Li$(p,n)^{7}$Be cross section at 3.5 MeV, and the charge collection. While the charge collection uncertainty was estimated to be 3.5% in Sec. II as a conservative value for absolute charge collection, here only the relative charge collection is needed, which likely means that this source of uncertainty is also greatly reduced. The results from the activation method are shown in Fig. 9 labeled as "Activation" and demonstrate generally good agreement with the angle-integrated cross section obtained from the prompt neutron measurement of the sum of the ^{6}Li(d,n_{0+1}) reactions, labeled as "This work", as measured with the ODeSA detectors. The activation results, with reduced uncertainties compared to the prompt neutron measurements, provided an independent confirmation of the absolute cross sections of the ^{6}Li(d,n) reaction.

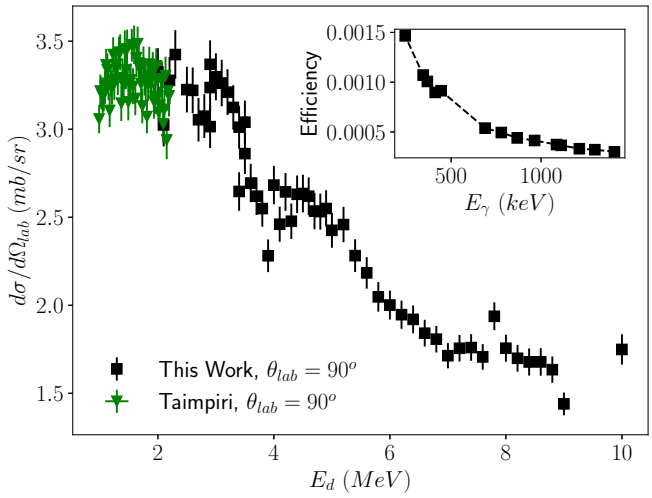

FIG. 10. Partial section for the ^{6}Li$(d,n_1\gamma)^{7}$Be reaction from this work. Measurements from Taimpiri *et al.* [45] are labeled as Taimpiri. The inset shows the absolute efficiency of a HPGe detector obtained from a calibrated ^{152}Eu source.

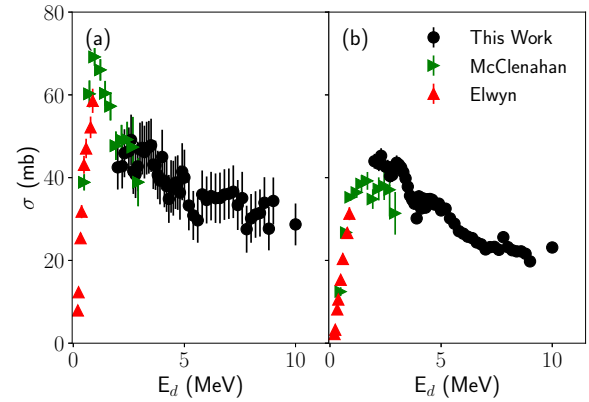

FIG. 11. Partial cross section for (a) the ^{6}Li$(d,n_0)^{7}$Be reaction, and (b) the ^{6}Li$(d,n_1)^{7}$Be reaction. The data from Elwyn *et al.* [1] and McClenahan and Segel [2] are labeled as Elwyn and McClenahan, respectively.

C. Gamma-ray angular distribution for ^{6}Li$(d,n_1)^{7}$Be

The ^{6}Li$(d,n_1)^{7}$Be reaction decays by emitting characteristic 429 keV γ rays from the $1/2^-$ first excited state into the $3/2^-$ ground state via an isotropic $M1$ transition [46]. The 429-keV secondary γ-ray yields were determined following the same procedure found in Sec. III A, and the systematic uncertainty on the γ-yield calculation was estimated to be 1%. The HPGe detectors were calibrated using a ^{152}Eu source to estimate the absolute detection efficiency with an uncertainty of 2.9%. The results from detector placed at 90° are only

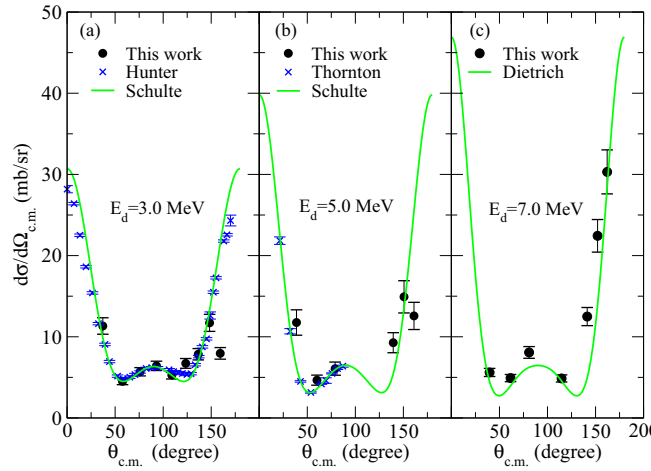

FIG. 12. Neutron angular distributions for the $d(d,n)^{3}$He reaction from this work at $E_d = 3.0$ (a), 5.0 (b), and 7.0 MeV (c) are compared to literature data labeled as Hunter [47] and Thornton [48]. The solid green lines are neutron angular distributions calculated using the Legendre coefficients from Schulte *et al.* [49] and Dietrich *et al.* [50].

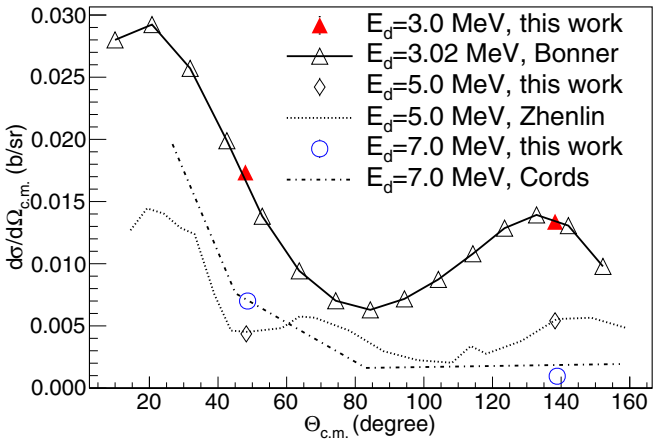

FIG. 13. Differential cross section for the ^{12}C$(d, p_0)\,^{13}$C reaction. The results from this work are compared with literature values labeled as Zhenlin [15], Cords [51], and Bonner [52].

presented in this work as the other two detectors were not functioning as expected during the experiment. The efficiency curve for a detector placed at 90° is shown in the Fig. 10 inset.

Figure 10 shows the partial cross section for ^{6}Li$(d, n_1)\,^7$Be determined from a detector placed at 90°. Differential cross sections below $E_d = 3.0$ MeV within the uncertainties are relatively flat, similar to the behavior reported by Taimpiri *et al.* [45]. The 429 keV γ-ray partial cross section for the ^{6}Li$(d, n_1)\,^7$Be reaction decreases with the increase in E_d above 3.0 MeV as shown in Fig. 10. The enhancement in cross sections at $E_d = 4$–5 MeV is due to additional contributions from broad $5/2^-$ states at the 6.7 and 7.2 MeV states in ^{7}Be. Also, the peak at $E_d = 7.8$ MeV is due to the additional contributions from the narrow $7/2^-$ state at 9.27 MeV in ^{7}Be.

The angle-integrated cross section for the ^{6}Li$(d, n_1)\,^7$Be reaction was determined by multiplying 429-keV γ-ray partial cross sections by 4π as shown in Fig. 11(b). Error bars on data from Ref. [2] are statistical only and an additional 15% uncertainty is reported in the publication. Although, our results for ^{6}Li$(d, n_1)\,^7$Be reaction are systematically higher compared to Ref. [2], they are still within the quoted systematic uncertainties. The angle-integrated ^{6}Li$(d, n_0)\,^7$Be cross section was then determined by subtracting the ^{6}Li$(d, n_1)\,^7$Be partial cross section from the ^{6}Li$(d, n_{0+1})\,^7$Be reaction cross section obtained from the ODeSA detectors as shown in Fig. 11(a).

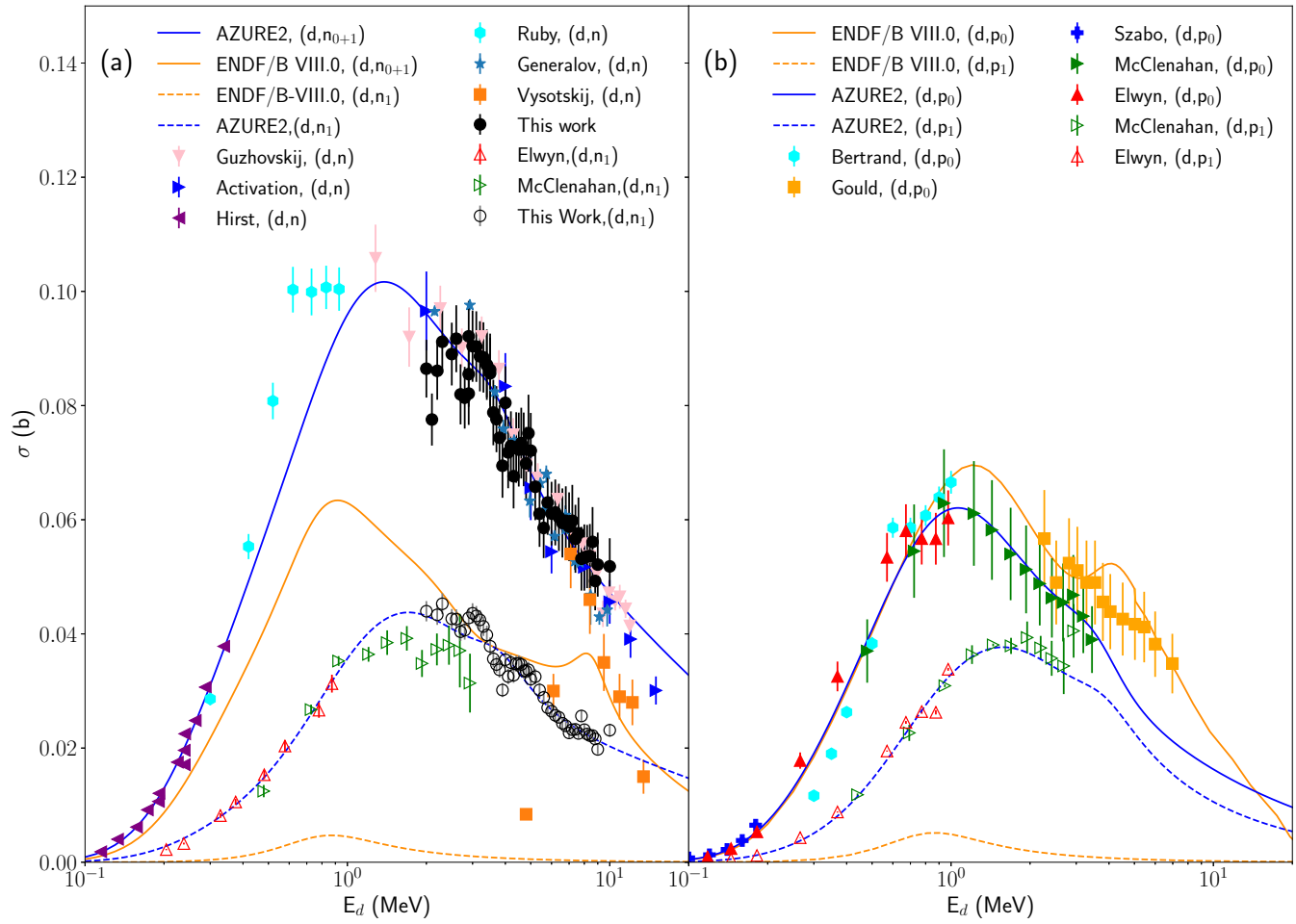

FIG. 14. Cross sections for (a) the ^{6}Li$(d, n_1)\,^7$Be and ^{6}Li$(d, n_{0+1})\,^7$Be reactions, and (b) the ^{6}Li$(d, p_0)\,^7$Li and the ^{6}Li$(d, p_1)\,^7$Li reactions. The cross sections are compared with *R*-matrix analyses using AZURE2 and the ENDF/B-VIII.0 evaluation.

These results were used for *R*-matrix analyses, which will be further discussed in Sec. III E.

D. $d(d, n)^{3}$He

The reference target, a CD_2 target, was studied to determine the $d(d, n)^{3}$He angular distributions for beam energies of $E_d = 3$, 5, and 7 MeV. The CD_2 target of thickness 200 μg/cm^2 (uncertainty of 5%) was prepared following Ref. [53]. The data analysis procedure is the same as that presented in Sec. III B. During the experimental campaign, the beam tune for $E_d = 5.0$ MeV changed so that the beam was hitting the Al frame in the target ladder, which was evident by increased γ-ray yields from the 1779-keV transition compared to those at $E_d = 3.0$ and 7.0 MeV. Thus, we also analyzed the ^{12}C$(d, p_0)^{13}$C reaction as a consistency check and to correct for the data taken at $E_d = 5.0$ MeV. The differential cross sections for the ^{12}C$(d, p_0)^{13}$C reaction, shown in Fig. 13, are consistent with literature values for $E_d = 3.0$ [52] and 7.0 MeV [51], but we overestimated for $E_d = 5.0$ MeV [15], as was the case for the $d(d, n)^{3}$He neutron angular distributions. A common correction factor applied to both $d(d, n)^{3}$He and ^{12}C$(d, p_0)^{13}$C cross sections at $E_d = 5.0$ MeV led to the consistent agreement between our results and the literature values in neutron detection and charged particle detection, as shown in Figs. 12 and 13. The angular distributions obtained from this work are compared with previous measurements [47–50] in Fig. 12. The green solid lines are the differential cross sections obtained using the Legendre coefficients adopted from Refs. [49,50]. The results from this work are in fair agreement with the literature values.

E. *R*-matrix analysis

With this comprehensive experimental data, we performed a multichannel *R*-matrix analysis using the AZURE2 code [54], as shown in Fig. 14. In the presented *R*-matrix analysis here, the normalizations of the experimental data sets were fixed to 1, so our results for ^{6}Li$(d, n_0)^{7}$Be and ^{6}Li$(d, p_0)^{7}$Li are expected to be different from ENDF/B-VIII.0. A forthcoming publication will describe the details of the *R*-matrix analysis and also explore the sensitivity of varying normalizations of data. Past measurements for the ^{6}Li$(d, n_0)^{7}$Be and ^{6}Li$(d, n_1)^{7}$Be reactions are reported below $E_d = 3.0$ MeV, and our results are consistent with the results from McClenahan and Segel [2]. For the ^{6}Li$(d, n_0)^{7}$Be and ^{6}Li$(d, n_1)^{7}$Be cross sections, our data extended the measurements up to $E_d = 10.0$ MeV, where they were previously lacking, and they were demonstrated to provide an additional constraint on the *R*-matrix analyses. The *R*-matrix fits to ^{7}Be production cross sections and ^{6}Li$(d, n_1)^{7}$Be partial cross sections are shown in Fig. 14(a). For the ^{6}Li$(d, p_0)^{7}$Li and ^{6}Li$(d, p_1)^{7}$Li reactions, our angular distribution data measured at 45° and 135° were included in the AZURE2 analyses, but only total cross section results were shown in Fig. 14(b) to directly compare with available literature data. The ENDF/B-VIII.0 evaluation does not include higher order partial waves ($\ell > 0$) and ^{6}Li$(d, n_1)^{7}$Be and ^{6}Li$(d, p_1)^{7}$Li data to constrain the fits to these partial cross sections, hence it produces negligible partial cross sections for excited state channels.

IV. CONCLUSIONS

Deuteron-induced reactions on a ^{6}Li target were measured in a self consistent way from $E_d = 1.8$ to 10 MeV with the angular coverage of 20°–170° in the laboratory frame of reference. Many of the reaction products, namely neutrons, γ rays, and charged particles, were detected simultaneously. The neutron angular distributions for ^{6}Li$(d, n_{0+1})^{7}$Be were reported from this measurement. The partial cross sections for ^{6}Li$(d, n_0)^{7}$Be and ^{6}Li$(d, n_1)^{7}$Be were reported for the first time at deuteron energies above 2 MeV, using a combination of direct neutron detection and secondary γ-ray transition detection for the (d, n_1) reaction. The results for the integrated cross section for the ^{6}Li$(d, n_{0+1})^{7}$Be reaction were found to be consistent with previous determinations. The uncertainties in the intrinsic efficiency of ODeSA neutron detectors are the dominant contribution to the overall uncertainty in our results. A precise measurement of the intrinsic efficiency and the detector response matrix is essential for better neutron spectroscopic measurements. An experimental campaign to measure the intrinsic efficiency of both ODeSA detectors and stilbene detectors is planned for the future at the Los Alamos Neutron Science Center using a white neutron source.

The 429-keV secondary γ rays from the ^{6}Li$(d, n_1\gamma)^{7}$Be reaction were detected to report the partial cross sections for ^{6}Li$(d, n_1)^{7}$Be for the first time up to $E_d = 10$ MeV. Our results are consistent with previous measurements in the overlapping deuteron beam energy region. The enhancement of ^{6}Li$(d, n_1)^{7}$Be partial cross sections at $E_d = 4$–5 MeV and at $E_d = 7.8$ MeV provide additional evidence for the existence of $5/2^-$ and $7/2^-$ states in ^{7}Be. The results for charged particle reaction channels, ^{6}Li$(d, d)^{6}$Li, ^{6}Li$(d, \alpha)\alpha$, and ^{6}Li$(d, p_{0,1})^{7}$Li, were also reported in this work, adding new experimental information on differential cross sections at energies where they were not observed before. The results from Generalov *et al.* [10,11] for ^{6}Li$(d, n_{0+1})^{7}$Be and charged particle channels were measured in two experimental campaigns. ^{6}Li$(d, n_{0+1})^{7}$Be cross sections were measured with the activation method with a systematic uncertainty of ≈2% [10] while the charged particle channels were measured with silicon detectors as in this work with a systematic uncertainty of 4%. The inconsistency observed between our results and results from Generalov *et al.* [10,11] for the charged particles could be related to different systematics from different experimental campaigns. Overall, our results are consistent with previous determinations with few exceptions and greatly expand on the existing range of the measured partial cross sections.

This work also demonstrated our ability to measure multiple reaction channels simultaneously in a self-consistent manner. We have demonstrated that systematic uncertainties could be better understood by analyzing all the reaction outputs simultaneously, and the detailed *R*-matrix analysis will benefit from these correlations to quantify final uncertainties. The additional data covering all of the reaction channels will better constrain the ongoing ^{8}Be evaluation effort, especially the partial cross sections for the ^{6}Li$(d, n_0)^{7}$Be, ^{6}Li$(d, n_1)^{7}$Be, ^{6}Li$(d, p_0)^{7}$Li, and ^{6}Li$(d, p_1)^{7}$Li reactions. These data were included in an *R*-matrix analysis of ^{8}Be

system using the AZURE2 [54] code as shown in Fig. 14. The full evaluation effort, which will include all the reaction channels and the full set of literature data is forthcoming in another publication. The results from this preliminary work already resolves the inconsistency explaining the ^{7}Be production data and the partial cross sections for $^{6}\mathrm{Li}(d,n_0)^{7}\mathrm{Be}$, $^{6}\mathrm{Li}(d,n_1)^{7}\mathrm{Be}$ highlighted in the Sec. I. For example, data from Hirst *et al.* [8] is ^{7}Be production data which in ENDF/B-VIII.0 evaluation was multiplied by a normalization factor of 0.6 to be interpreted as the $^{6}\mathrm{Li}(d,n_0)^{7}\mathrm{Be}$ partial cross section.

High fidelity, self consistent data sets produced by correlating output reaction products can serve to fill the gap in nuclear data, reduce the discrepancies among different evaluations, and avoid applying multiple normalization factors on different facilities' measurements. The simultaneous measurement of all reaction products from an experiment avoids the need of multiple normalization factors to each reaction channel in evaluation of the data. In addition, any spectroscopic information, neutron- and γ-ray yields from the reaction, and angular distributions suggest information to validate transport Monte Carlo codes as a new practical use. One approach to utilize this type of experimental capability is to provide better differential data for (α, n) reactions on light nuclei for nuclear applications.

ACKNOWLEDGMENTS

This work was performed under the National Nuclear Security Administration of the U.S. Department of Energy at Los Alamos National Laboratory under Contract No. 89233218CNA000001. This work benefits from the LANSCE accelerator facility and the Institute for Structure and Nuclear AstroPhysics (ISNAP) at the University of Notre Dame. This research utilized resources from the Notre Dame Center for Research Computing and was supported by the National Science Foundation through Grants No. PHY-2011890 and No. PHY-2310059 (University of Notre Dame Nuclear Science Laboratory) and Grant No. PHY-1430152 (the Joint Institute for Nuclear Astrophysics–Center for the Evolution of the Elements).

[1] A. J. Elwyn, R. E. Holland, C. N. Davids, L. Meyer-Schutzmeister, J. E. Monahan, F. P. Mooring, and W. Ray, Phys. Rev. C **16**, 1744 (1977).
[2] C. R. McClenahan and R. E. Segel, Phys. Rev. C **11**, 370 (1975).
[3] G. Bertrand, G. Grenier, and J. Pornet, CEN Saclay Report No. 3428, Centre d'Etudes de Limeil, Villeneuve-Saint-Georges, France, 1968.
[4] C. R. Could, J. M. Joyce, and J. R. Boyce, *Nuclear Cross Sections and Technology, Volume II. Proceedings of a Conference*, (National Bureau of Standards, Washington, 1975), p. 697.
[5] J. Szabó, Z. Bödy, S. Szegedi, and M. Várnagy, Nucl. Phys. A **289**, 526 (1977).
[6] L. Ruby, R. V. Pyle, and Y.-C. Wong, Nucl. Sci. Eng. **71**, 280 (1979).
[7] B. J. Guzhovskij, S. N. Abramovich, A. G. Zvenigo-rodskij, G. N. Slepcov, and S. V. Trusillo, Izv. Ross. Akad. Nauk Ser. Fiz. **44**, 168 (1980).
[8] F. Hirst, I. Johnstone, and M. Poole, London Edinburgh Dublin Philos. Mag. J. Sci. **45**, 762 (1954).
[9] Haouat (1985), received by G. Hale through Priv. Comm. with the author.
[10] L. N. Generalov, S. N. Abramovich, and S. M. Selyankina, Izv. Ross. Akad. Nauk Ser. Fiz. **81**, 717 (2017).
[11] L. N. Generalov, O. P. Vikhlyantsev, I. A. Karpov, A. V. Kuryakin, A. D. Tumkin, S. V. Fil'chagin, and D. A. Fedotov, Bull. Russ. Acad. Sci. Phy. **84**, 717 (2020).
[12] S. N. Abramovich, B. Y. Guzhovskii, B. M. Dzyuba, A. G. Zvenigorodskii, S. V. Trusillo, and G. N. Sleptsov, Izv. Akad. Nauk SSR Ser. Fiz. **40**, 842 (1976).
[13] D. Powell, G. Crawley, B. Rao, and B. Robson, Nucl. Phys. A **147**, 65 (1970).
[14] Y. Rongfang, W. Zhifu, Y. Binqi, S. Zuxun, and Y. Jian, Chin. J. Nucl. Phys. **3**, 155 (1981).
[15] M. Zhenlin, Z. Youxiang, S. Zuxun, Z. Peihua, W. Zhifu, Y. Jian, Y. Rongfang, and W. Keling, in Conference on Low Energy Physics, Lanzhou, 1972 (unpublished).
[16] H. Bingham, A. Zander, K. Kemper, and N. Fletcher, Nucl. Phys. A **173**, 265 (1971).
[17] G. Bruno, J. Decharge, A. Perrin, G. Surget, and C. Thibault, J. Phys. France **27**, 517 (1966).
[18] R. Risler, W. Grüebler, A. Debenham, V. König, P. Schmelzbach, and D. Boerma, Nucl. Phys. A **286**, 115 (1977).
[19] P. Paul and K. Lieb, Nucl. Phys. **53**, 465 (1964).
[20] V. Meyer, W. Pfeifer, and H. H. Staub, Helv. Phys. Acta **36**, 465 (1963).
[21] H. Bingyin, S. Zuxun, Z. Youxiang, Z. Peihua, W. Xinlin, W. Zhifu, Y. Jian, and Y. Rongfang, in Conference on Nuclear Physics, Shanghai, 1974 (unpublished).
[22] E. Ntemou, X. Aslanoglou, M. Axiotis, V. Foteinou, M. Kokkoris, A. Lagoyannis, P. Misaelides, N. Patronis, K. Preketes-Sigalas, G. Provatas, and R. Vlastou, Nucl. Instrum. Methods Phys. Res., Sect. B **407**, 34 (2017).
[23] J. P. Schiffer, G. C. Morrison, R. H. Siemssen, and B. Zeidman, Phys. Rev. **164**, 1274 (1967).
[24] V. Singh, D. Bhowmick, and D. Basu, Astropart. Phys., **162** 102995 (2024).
[25] I. Cook, N. P. Taylor, and D. J. Ward, in *20th IEEE/NPSS Symposium on Fusion Engineering, 2003* (IEEE, Piscataway, NJ, 2003), pp. 39–44.
[26] D. Fasel and M. Tran, Fusion Eng. Des. **75-79**, 1163 (2005).
[27] D. Brown, M. Chadwick, R. Capote, A. Kahler, A. Trkov, M. Herman, A. Sonzogni, Y. Danon, A. Carlson, M. Dunn, D. Smith, G. Hale, G. Arbanas, R. Arcilla, C. Bates, B. Beck, B. Becker, F. Brown, R. Casperson, J. Conlin *et al.*, Nucl. Data Sheets **148**, 1 (2018).
[28] I. Thomson, Charged particle evaluations, plans for post - ENDF/B-VIII.0, 2017, https://indico.bnl.gov/event/3580/contributions/10522/.
[29] A. M. Lane and R. G. Thomas, Rev. Mod. Phys. **30**, 257 (1958).
[30] P. Pereslavtsev, U. Fischer, S. Simakov, and M. Avrigeanu, Nucl. Instrum. Methods Phys. Res., Sect. B **266**, 3501 (2008).

[31] N. Otuka, E. Dupont, V. Semkova, B. Pritychenko, A. Blokhin, M. Aikawa, S. Babykina, M. Bossant, G. Chen, S. Dunaeva, R. Forrest, T. Fukahori, N. Furutachi, S. Ganesan, Z. Ge, O. Gritzay, M. Herman, S. Hlavač, K. Katō, B. Lalremruata *et al.*, Nucl. Data Sheets **120**, 272 (2014).
[32] P. R. Page, Phys. Rev. C **72**, 054312 (2005).
[33] M. Febbraro, R. Toomey, S. Pain, K. Chipps, B. Becker, R. Newby, Z. Meisel, T. Massey, C. Brune, Q. Liu, R. deBoer, K. Macon, A. Boeltzig, J. O'Neill, M. Smith, M. Wiescher, D. Soltesz, I. Sultana, K. Brandenburg, S. Subedi *et al.*, Nucl. Instrum. Methods Phys. Res., Sect. A **946**, 162668 (2019).
[34] N. Fotiades, G. D. Johns, R. O. Nelson, M. B. Chadwick, M. Devlin, W. S. Wilburn, P. G. Young, J. A. Becker, D. E. Archer, L. A. Bernstein, P. E. Garrett, C. A. McGrath, D. P. McNabb, and W. Younes, Phys. Rev. C **69**, 024601 (2004).
[35] N. Fotiades, R. O. Nelson, and M. Devlin, Phys. Rev. C **81**, 037304 (2010).
[36] J. Becker, L. Bernstein, W. Younes, D. McNabb, P. Garrett, D. Archer, C. McGrath, M. Stoyer, H. Chen, W. Ormand, R. Nelson, G. Chadwick, M.B. adn Johns, D. Drake, P. Young, M. Devlin, N. Fotiades, and W. Wilburn, J. Nucl. Sci. Technol. **39**, 620 (2002).
[37] J. A. Becker and R. O. Nelson, AIP Conf. Proc. **769**, 748 (2005).
[38] L. N. Generalov, V. A. Zherebtsov, and S. M. Selyankina, Bull. Russ. Acad. Sci. Phys. **86**, 937 (2022).
[39] M. Febbraro, B. Becker, R. deBoer, K. Brandenburg, C. Brune, K. Chipps, T. Danley, A. D. Fulvio, Y. Jones-Alberty, K. Macon, Z. Meisel, T. Massey, R. Newby, S. Pain, S. Paneru, S. Shahina, M. Smith, D. Soltesz, S. Subedi, I. Sultana *et al.*, Nucl. Instrum. Methods Phys. Res., Sect. A **989**, 164824 (2021).
[40] O. N. Vysotskij, O. K. Gorpinich, V. S. Zaritskij, S. N. Kondratyev, V. S. Prokopenko, S. B. Rakitin, V. D. Sklyarenko, V. A. Stepanenko, and V. V. Tokarevskij, in Conference on Nuclear Spectroscopy and Nuclear Strucure, Leningrad, 1990 (unpublished).
[41] T. N. Massey, D. K. Jacobs, S. I. Al-Quraishi, S. M. Grimes, C. E. Brient, W. B. Howard, and J. C. Yanch, J. Nucl. Sci. Technol. **39**, 677 (2002).
[42] J. W. Meadows, Nucl. Instrum. Methods Phys. Res., Sect. A **324**, 239 (1993).
[43] Q. Liu, M. Febbraro, R. Deboer, S. Aguilar, A. Boeltzig, Y. Chen, M. Couder, J. Görres, E. Lamere, S. Lyons, K. Macon, K. Manukyan, L. Morales, S. Pain, W. Peters, C. Seymour, G. Seymour, R. Toomey, B. V. Kolk, J. Weaver *et al.*, Phys. Rev. C **101**, 025808 (2020).
[44] H. Liskien and A. Paulsen, At. Data Nucl. Data Tables **15**, 57 (1975).
[45] E. Taimpiri, M. Axiotis, K. Bosmpotinis, M. Kokkoris, A. Lagoyannis, and A. Ziagkova, Nucl. Instrum. Methods Phys. Res., Sect. B **539**, 162 (2023).
[46] R. Evans, *The Atomic Nucleus* (McGraw Hill, New York, 1955), p. 235.
[47] G. T. Hunter and H. T. Richards, Phys. Rev. **76**, 1445 (1949).
[48] S. Thornton, Nucl. Phys. A **136**, 25 (1969).
[49] R. Schulte, M. Cosack, A. Obst, and J. Weil, Nucl. Phys. A **192**, 609 (1972).
[50] F. Dietrich, E. Adelberger, and W. Meyerhof, Nucl. Phys. A **184**, 449 (1972).
[51] H. Cords, G. Din, and B. Robson, Nucl. Phys. A **127**, 95 (1969).
[52] T. W. Bonner, J. T. Eisinger, A. A. Kraus, and J. B. Marion, Phys. Rev. **101**, 209 (1956).
[53] M. Febbraro, D. Walter, S. Shadrick, S. Pain, K. Chipps, C. Thornsberry, and E. Lesser, Nucl. Instrum. Methods Phys. Res., Sect. B **410**, 53 (2017).
[54] R. E. Azuma, E. Uberseder, E. C. Simpson, C. R. Brune, H. Costantini, R. J. de Boer, J. Görres, M. Heil, P. J. LeBlanc, C. Ugalde, and M. Wiescher, Phys. Rev. C **81**, 045805 (2010).